Observer-based active damping for grid-connected converters with LCL filter

Observer-based active damping for grid-connected converters with LCL filter

Y. Zhang*, M. G. L. Roes, M. A. M. Hendrix and J. L. Duarte
Department of Electrical Engineering
Eindhoven University of Technology
P.O. Box 513, 5600MB Eindhoven, The Netherlands
*E-mail: ya.zhang@tue.nl

***Abstract*—In this paper an add-on control method is proposed to damp oscillations in the LCL filter of a grid-connected converter. An observer is used to estimate the capacitor current, and successively, a conventional active damping technique is applied. Since the capacitor current is estimated from already available measurements, the proposed active damping method does not need an extra current sensor for the capacitor current. Model analysis and simulation validate the effectiveness of the proposed control method.**

***Keywords*—observer, damping, converter, LCL filter, control**

I. Introduction

Pulse width modulation (PWM) converters are widely applied to interface sustainable energy sources, the public grid and local loads [1]–[4]. Because of their good trade-off between attenuating performance and the filter size, LCL filters are widely employed to attenuate PWM switching frequency harmonics [5], [6]. However, the LCL filter also introduces unwanted oscillations at its resonance frequency. Passive damping [7] can reduce these oscillations efficiently but is undesired since it comes at the cost of reduced power efficiency. Active damping [8], [9] is more advantageous because no actual power losses are generated.

Most active damping techniques need the measurements of the capacitor current or voltage, which adds to the system's total hardware cost. In this paper an observer-based active damping technique is presented. It estimates the capacitor current from the LCL filter model and the already existing measurements of the converter output current and the output voltage. Conventional capacitor current based active damping techniques can then be applied to damp the filter's resonance.

II. Observer-based active damping

A simplified model for a single-phase grid connected converter with LCL filter is shown in Fig. 1, where the proposed add-on active damping technique is indicated in the dashed box. The converter output current and the voltage at the point of common connection (pcc) are used for the capacitor current estimation. Additionally, a high-pass filter (HPF) is applied. This section introduces the algorithm of the proposed damping method.

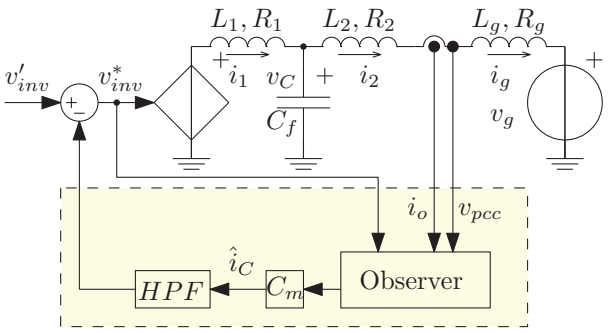

Fig. 1. Proposed observer-based active damping technique applied to a grid-connected converter with LCL filter

A. Modelling

The LCL filter dynamics in Fig. 1 are described by three differential equations, given by

$$\begin{aligned} L_1\frac{\mathrm{d}}{\mathrm{d}t}i_1(t) =& - R_1 i_1(t) - v_C(t) + v^*_{inv}(t) \\ C_f\frac{\mathrm{d}}{\mathrm{d}t}v_C =& i_1(t) - i_2(t) \\ L_2\frac{\mathrm{d}}{\mathrm{d}t}i_2(t) =& v_C(t) - R_2 i_2(t) - v_{pcc}(t), \end{aligned} \tag{1}$$

where i_1, v_c and i_2 are the current through L_1, capacitor voltage and the output current, respectively. A state-space model [10] for the plant in (1) is

$$\begin{aligned} \dot{x}(t) =& Ax(t) + Bu(t) + E\omega(t) \\ y(t) =& Cx(t), \end{aligned} \tag{2}$$

with

$$A = \begin{bmatrix} \frac{-R_1}{L_1} & \frac{-1}{L_1} & 0 \\ \frac{1}{C_f} & 0 & \frac{-1}{C_f} \\ 0 & \frac{1}{L_2} & \frac{-R_2}{L_2} \end{bmatrix}, B = \begin{bmatrix} \frac{1}{L_1} \\ 0 \\ 0 \end{bmatrix}, E = \begin{bmatrix} 0 \\ 0 \\ \frac{-1}{L_2} \end{bmatrix},$$
$$C = \begin{bmatrix} 0 & 0 & 1 \end{bmatrix}, \tag{3}$$

and the state variables, input, disturbance, and output respectively represent

$$\begin{aligned} x(t) =& \begin{bmatrix} i_1(t) & v_C(t) & i_2(t) \end{bmatrix}^T, \\ u(t) =& v^*_{inv}(t),\ \omega(t) = v_{pcc}(t),\ y(t) = i_o(t). \end{aligned} \tag{4}$$

The *zero order hold* method is applied to obtain the discrete-time model for the plant in (2). Accordingly, we have

$$\begin{aligned} x[k+1] =& A_d x[k] + B_d u[k] + E_d \omega[k] \\ y[k] =& C_d x[k], \end{aligned} \tag{5}$$

where $x[k]$, $u[k]$, $\omega[k]$ and $y[k]$ represent the sampled data state variables, input, disturbance, and output in (2). A_d, B_d, E_d and C_d are the resulting matrices from discretization of A, B, E and C.

B. Observer: estimation of capacitor current

The observer in this paper uses the plant model for state estimation [11]. It is described by

$$\begin{aligned} \hat{x}[k+1] =& A_d \hat{x}[k] + B_d u[k] + E_d \omega[k] \\ &+ L_{ob}(y[k] - C_d \hat{x}[k]), \end{aligned} \tag{6}$$

where $\hat{x}[k]$ is the estimate of $x[k]$ and L_{ob} is the observation gain vector/matrix. Since in Fig. 1 $i_C = i_1 - i_2$ holds according to *Kirchhoff's current law*, the estimate of the capacitor current is obtained from

$$\hat{i}_C[k] = C_m \hat{x}[k], \tag{7}$$

with $C_m = \begin{bmatrix} 1 & 0 & -1 \end{bmatrix}$.

C. High-pass filter for active damping

Placing a resistor in series with the capacitor effectively yields passive damping; the damping performance could be theoretically maintained by using a high-pass filter feeding back the capacitor current to the input voltage [12]. However, to resolve delays due to PWM, data sampling and computation, as addressed in [13], a modification is made to the high-pass filter. The filter employed in this paper is

$$K_{hpf}(s) = K_v K(s), \tag{8}$$

where K_v is a gain for tuning and $K(s)$ is from [12], described by

$$K(s) = \frac{R_v C_f L_2 s^2}{C_f L_2 s^2 + C_f R_v s + 1}. \tag{9}$$

The parameters C_f and L_2 are the capacitance and inductance indicated in Fig. 1, and R_v is a *virtual resistor* [12] used to achieve the desired passive damping performance.

III. Validation of the Converter Modelling

Since the estimation of the capacitor current is based on the derived model of the grid-connected converter with LCL filter in (5), it is of vital importance to have an effective model. The outputs of the derived model are compared to the measurements, following the schematics shown in Fig. 2, where the derived plant model in (5) is implemented as indicated in the red dashed box. The circuit and the model are compared under two conditions: weak grid condition and stiff grid condition. In both scenarios, a 10% third harmonic (with respect to the fundamental) is added to the grid voltage at 0.107s to trigger transient behaviour. The grid voltage waveform is shown in Fig. 3. The parameters of the LCL filter in these tests are listed in Table I and the sampling rate is 20 kHz.

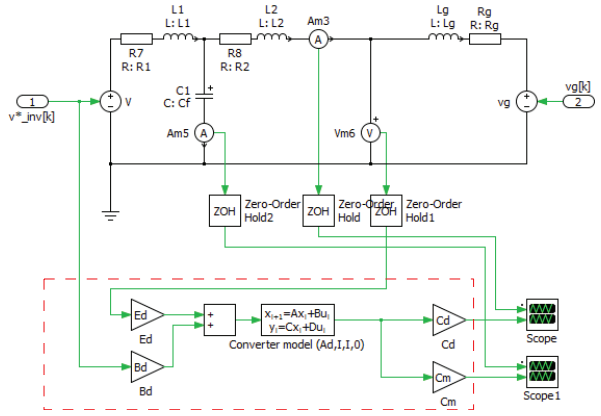

Fig. 2. Schematic in PLECS used to check the derived state space model.

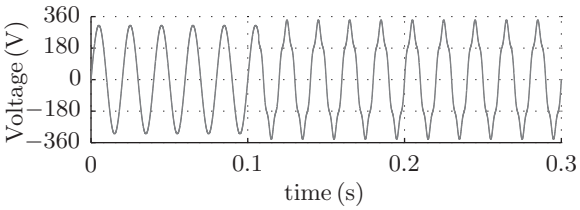

Fig. 3. Waveform of the grid voltage v_g applied to trigger transient behaviour.

A. Weak grid condition

A weak grid condition is created by setting $L_g = 10.44\,\text{mH}$. The capacitor current waveforms from the circuit and from the state space model are shown in Fig. 4. It can be seen that the oscillation of the LCL filter clearly presents in the response of the derived model under the weak grid condition.

B. Stiff grid condition

A stiff grid condition is created by setting $L_g = 0.1\,\text{mH}$. The capacitor current waveforms from the circuit and from the state space model in (5) are shown in Fig. 5.

The difference between the current waveforms from the model (the plant model in (5)) and the circuit (in Fig. 2) can be explained by the delays involved by using zero-order-hold. In an extreme case when the sampling rate is infinite, the derived model should be equivalent to the circuit. In the derived model, the information of the PCC voltage is delayed due to the zero-order-hold block applied (Fig. 2).

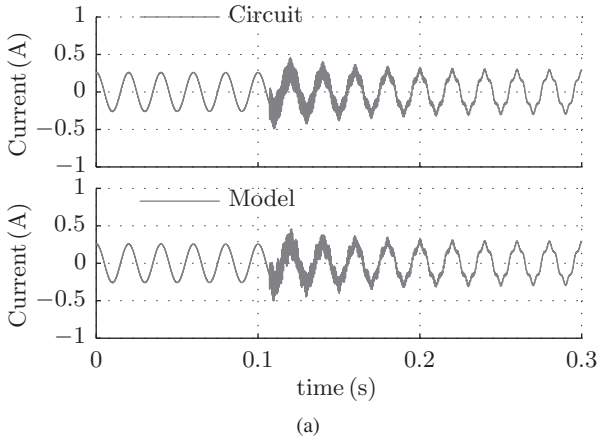

(a)

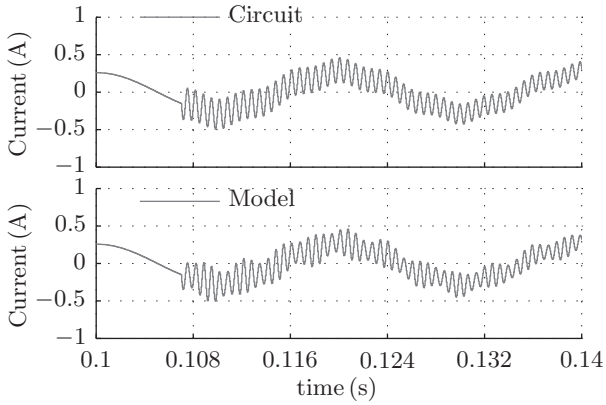

(b)

Fig. 4. Capacitor current waveforms from the circuit and from the state space model in (5) under weak grid condition: (a) zoomed-out view ; (b) zoomed-in view.

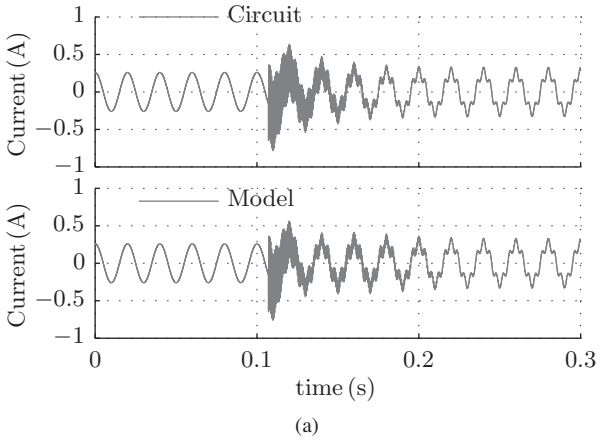

(a)

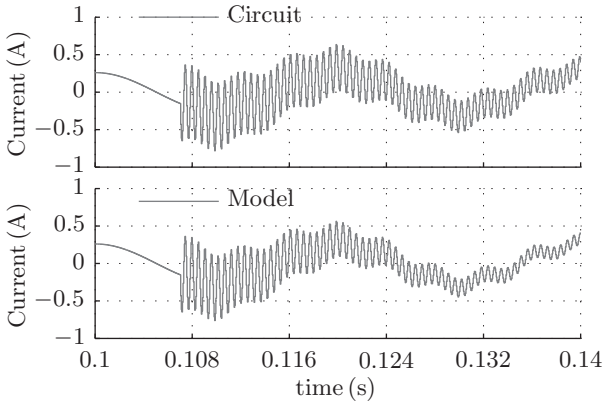

(b)

Fig. 5. Capacitor current waveforms from the circuit and from the state space model under stiff grid condition: (a) zoomed-out view ; (b) zoomed-in view.

IV. Analysis of the Active Damping Technique

In theory the high-pass filter feedback in (8) yields stable resonance damping even without tuning ($K_v = 1$). However, instability may occur due to the delays introduced by the digital implementation [14]. In light of this, stability analysis is performed in this section.

A. Open-loop damping gain

Synthesizing the plant model in (5) and the observer in (6), the state space model from the voltage v^*_{inv} and the pcc voltage v_{pcc} to the estimated capacitor current is

$$\begin{bmatrix} x[k+1] \\ e[k+1] \end{bmatrix} = \underbrace{\begin{bmatrix} A_d & O \\ O & A_d - L_{ob}C_d \end{bmatrix}}_{\bar{A}_d} \begin{bmatrix} x[k] \\ e[k] \end{bmatrix} + \underbrace{\begin{bmatrix} B_d \\ O \end{bmatrix}}_{\bar{B}_d} u[k] + \underbrace{\begin{bmatrix} E_d \\ O \end{bmatrix}}_{\bar{E}_d} \omega[k]$$

$$\hat{i}_C[k] = \underbrace{\begin{bmatrix} C_m & -C_m \end{bmatrix}}_{\bar{C}_d} \begin{bmatrix} x[k] \\ e[k] \end{bmatrix}, \tag{10}$$

where $e[k]$ is the state estimation error, denoted as $e[k] = x[k] - \hat{x}[k]$. It can be seen from (10) that the estimation error is uncontrollable; however, it is stabilizable since the eigenvalue of $A_d - L_{ob}C_d$ can be relocated with proper design of the observation gain vector/matrix L_{ob}. The open loop transfer function from the inverter output voltage to the estimated capacitor current is

$$G(z) = \frac{\hat{i}_C(z)}{v^*_{inv}(z)} = \bar{C}_d(zI - \bar{A}_d)\bar{B}_d. \tag{11}$$

It is suggested that during stability analysis $1.5T_s$ delay should be accounted for PWM, data sampling and computation [14], where T_s is the sampling period. Since fractional-order delay adds to the complexity of stability analysis in the z-domain, this section approximates the worst case delay by 2 sampling periods. Therefore, the open loop gain of the damping path is

$$T(z) = K_{hpf}(z)G(z)z^{-2}, \tag{12}$$

where $K_{hpf}(z)$ is the discrete-time implementation of $K_{hpf}(s)$ in (8). Combination of (8) and (12) yields

$$T(z) = K_v K(z)G(z)z^{-2}. \tag{13}$$

It is worth mentioning that two parameters can be tuned in the design of the observer-based active damping: K_v and R_v. The discussion of these two parameters follows in the next sections.

B. Nyquist plot of $T(z)$

Table I lists the parameters of the considered LCL filter. The observer gain vector/matrix L_{ob} is designed in such a way that it can track the plant state variables in $0.2T_g$, where T_g is the grid period. The roots of Bessel Polynomials are adopted as locations of the eigenvalues of $A_d - L_{ob}C_d$. The sampling frequency is chosen as $f_s = 20\,\text{kHz}$. Accordingly, the Nyquist plots of $T(z)$ with different values of R_v are shown in Fig. 6; the tuning gain is set as $K_v = 0.25$ for stability.

As can be seen from Fig. 6, increasing R_v decreases the gain margin; nevertheless, the phase margin increases. Moreover, setting the tuning gain $K_v = 1$ can make the system unstable, referring to the plot with $R_v = 100$ in Fig. 6 (where $K_v = 0.25$ is used).

TABLE I. LCL FILTER PARAMETERS

Description	Symbol	Value
Converter side inductor	L_1,R_1	5.22 mH,0.2 Ω
Capacitor	C_f	2.82 μF
Grid side inductor	L_2,R_2	5.22 mH,0.2 Ω

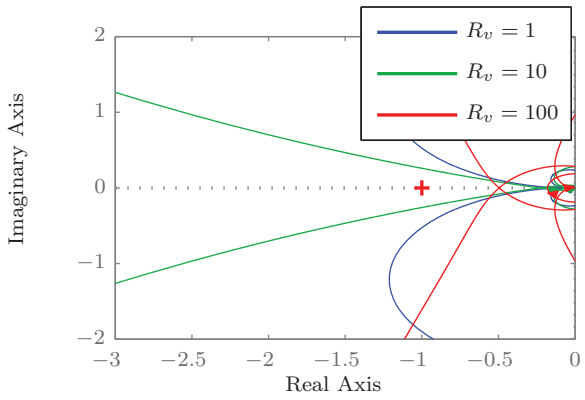

Fig. 6. Nyquist plot of $T(z)$, with different values of R_v, and $K_v = 0.25$.

C. Closed-loop damped plant model

The closed-loop transfer function from v'_{inv} to the converter output current i_o (with reference to Fig. 1) is found to be

$$\bar{P} = \frac{i_o(z)}{v'_{inv}(z)} = \frac{P(z)}{1 + T(z)}, \tag{14}$$

where $P(z)$ is the undamped plant transfer function, described by $P(z) = C_d(zI - A_d)B_d$ according to the undamped plant model in (5).

D. Bode plot of $\bar{P}(z)$

Fig. 7 shows the Bode plots of the damped plant with different values of R_v, with the tuning factor $K_v = 0.25$. It can be seen that increasing the value of R_v yields more damping of the LCL filter resonance.

Fig. 8 shows the Bode plots of the damped plant with different values of K_v, with $R_v = 100$. It can be seen that increasing the value of K_v gives more damping to the LCL filter resonance as well; however, it may make the plant unstable, as depicted in Fig. 6.

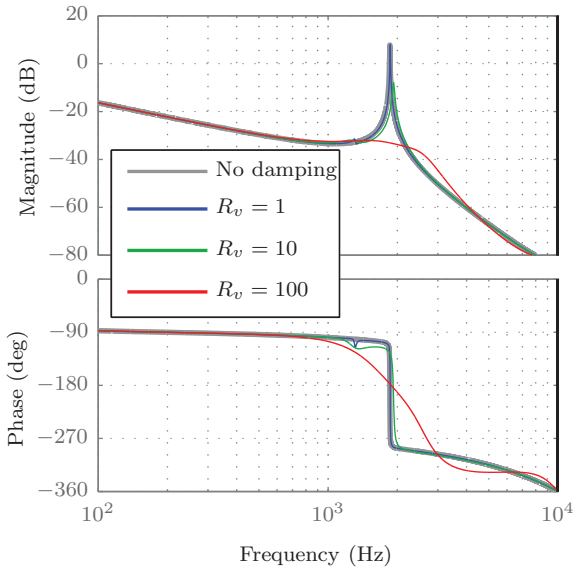

Fig. 7. Bode plot of $\bar{P}(z)$ to show the benefit of active damping, with different values of R_v, and $K_v = 0.25$.

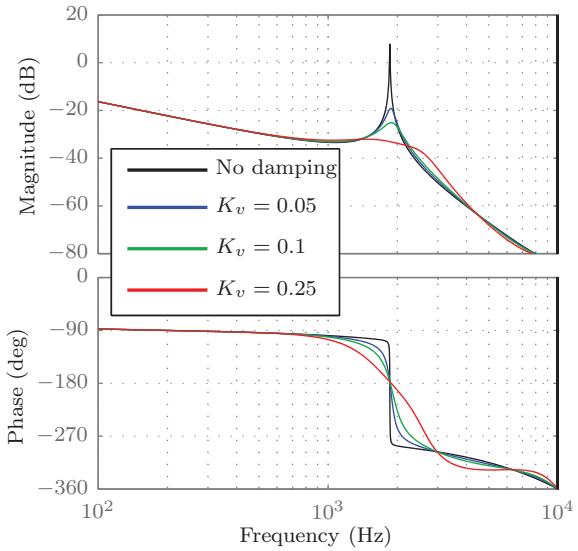

Fig. 8. Bode plot of $\bar{P}(z)$ to show the benefit of active damping, with different values of K_v, and $R_v = 100$.

For a good trade-off between stability margins and LCL filter resonance attenuation effect, $R_v = 100$ and $K_v = 0.25$ are chosen for the active damping design, as summarized in Table II.

V. PR CURRENT CONTROLLER

In this section, a proportional-resonance (PR) current controller is considered to regulate the converter output current. The transfer function of the PR control in the s-domain is

$$G_{pr}(s) = K_p + K_r \frac{s}{s^2 + \omega_o^2}, \tag{15}$$

where K_p is the proportional gain, K_r the resonance gain, and ω_0 is the grid angular frequency. The parameters for the PR control are listed in Table II. The PR is discretized using *forward Euler* and *Backward Euler* methods as in [15] to avoid algebraic loops. The resulting PR control in discrete form is denoted as $G_{pr}(z)$. Ignoring the dynamics caused by the PCC voltage change (with reference to Fig. 1), the closed loop transfer function of the PR current controlled converter is

$$G_{cl}(z) = \frac{\bar{P}(z)G_{pr}(z)z^{-2}}{1 + \bar{P}(z)G_{pr}(z)z^{-2}}, \tag{16}$$

where z^{-2} is introduced to account for delays ($2T_s$). Fig. 9 shows the Nyquist plots of $\bar{P}(z)G_{pr}(z)z^{-2}$ with and without active damping. Consistent with the observation in Fig. 7 and Fig. 8, applying the proposed active damping technique helps to stabilize the current control feedback system.

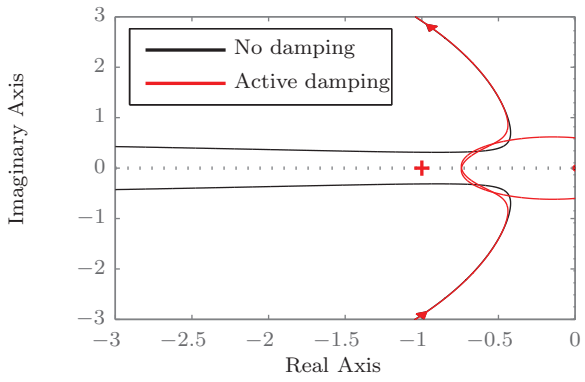

Fig. 9. Nyquist plot of $\bar{P}(z)G_{pr}(z)z^{-2}$ with and without active damping

TABLE II. PARAMETERS OF THE CONTROLLER

Description	Symbol	Value
PR filter	K_p	30
	K_r	6000
	ω_0	$2\pi f_g$
Active damping	K_v	0.25
	R_v	100
Sampling	f_s	20 kHz

VI. SIMULATION RESULTS

Two sets of simulation tests were performed in *Matlab/Simulink/Plecs* to investigate the aforementioned stability discussion. A full bridge converter is used with a 400 V DC input source. A unipolar pulse-width-modulation scheme is applied to the full bridge converter. The switching frequency is $f_{sw} = 20\,\text{kHz}$ and the desired peak output current is set as 4 A. The LCL filter parameters in simulation are shown in Table I.

A. Weak grid condition

A weak grid condition is created by setting $L_g = 10.44\,\text{mH}$, with reference to the circuit in Fig. 1. Figure 10, Figure 11 and Figure 12 show the simulated transient waveforms of the converter output current i_o under the weak grid condition. In Fig. 10 the active damping loop is disabled at 0.1 s by setting K_v to zero. In Fig. 11 at 0.1 s the parameter K_v is set from 0.25 to 1, and in Fig. 12 at 0.1 s the parameter K_v is set from 0.25 to 2.

It can be seen that the system becomes unstable when the observer-based active damping is disabled in Fig. 10, which is in agreement with the analysis of Fig. 9. Moreover, in accordance with the results in Fig. 6, in Fig. 11 and Fig. 12 it is shown that a large K_v can also make the system unstable.

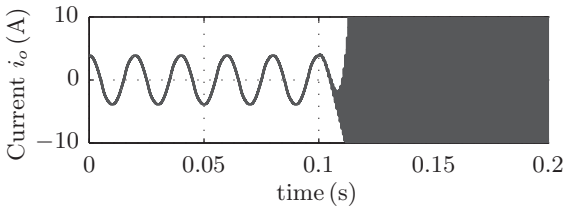

Fig. 10. Simulated transient response of i_o at the weak grid condition. The active damping is disabled at 0.1 s by setting K_v from 0.25 to zero.

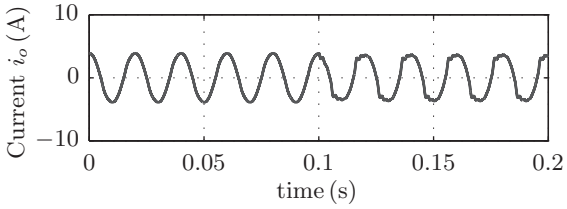

Fig. 11. Simulated transient response of i_o at the weak grid condition. At 0.1 s the parameter K_v is set from 0.25 to 1.

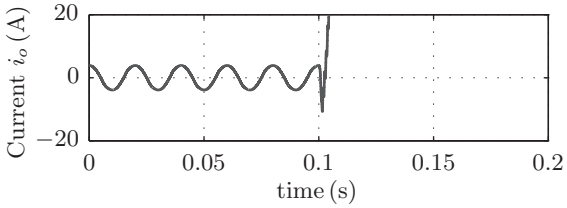

Fig. 12. Simulated transient response of i_o at the weak grid condition. At 0.1 s the parameter K_v is set from 0.25 to 2.

B. Stiff grid condition

A stiff grid condition is created by setting $L_g = 0.1\,\text{mH}$, with reference to the circuit in Fig. 1. Figure 13, Figure 14 and Figure 15 show the simulated transient waveforms of the converter output current i_o under the stiff grid condition. In Fig. 10 the active damping loop is disabled at 0.1 s by setting K_v to zero. In Fig. 14 at 0.1 s

the parameter K_v is set from 0.25 to 1, and in Fig. 15 at $0.1\,\mathrm{s}$ the parameter K_v is set from 0.25 to 2.

Consistent with under the weak grid condition, the system becomes unstable when the active damping is disabled. This is as expected since no grid parameter is used for the observer design. Moreover, an un-decaying harmonic oscillation present in the converter output current waveform when K_v increases to 1 (in Fig. 14) and in a worse case the system becomes unstable (in Fig. 15), which is also consistent with under the weak grid condition.

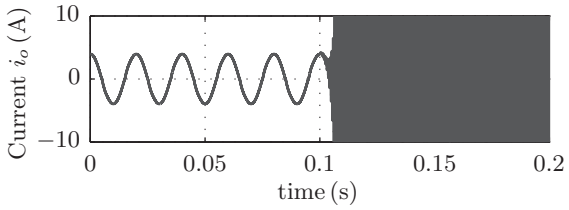

Fig. 13. Simulated transient response of i_o at the stiff grid condition. The active damping is disabled at $0.1\,\mathrm{s}$ by setting K_v from 0.25 to zero.

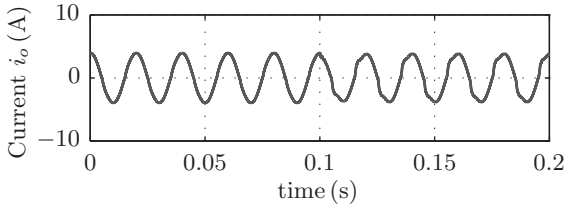

Fig. 14. Simulated transient response of i_o at the stiff grid condition. At $0.1\,\mathrm{s}$ the parameter K_v is set from 0.25 to 1.

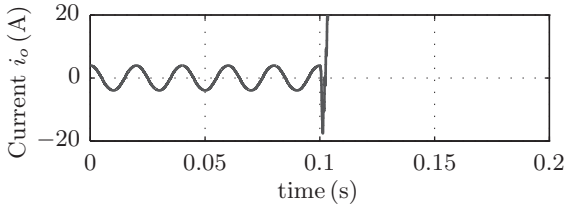

Fig. 15. Simulated transient response of i_o at the stiff grid condition. At $0.1\,\mathrm{s}$ the parameter K_v is set from 0.25 to 2.

VII. Conclusion

In this paper an add-on control scheme is proposed to damp the resonance of the LCL filter. It estimates the capacitor current from the measurements of the grid-side converter output current, the local voltage, and the LCL filter parameters. Accordingly, a conventional capacitor-current-based active damping technique can be applied. The advantage of this scheme is that there is no need to measure the capacitor current, making it an add-on feature for grid-connected converters since the measurement of the output current and local voltage already exist. A model is derived to define the stability region of the proposed active damping technique.

In order to validate the damping benefit provided by the proposed control technique, a proportional-resonance current controller is added to the grid-connected converter. The overall system is shown to be stable with the damping technique and unstable without. On top of that, simulation results show that the active damping technique is applicable for both weak and stiff grid operation.

References

[1] F. Wang, J. L. Duarte, M. A. M. Hendrix, and P. F. Ribeiro, "Modeling and analysis of grid harmonic distortion impact of aggregated DG inverters," *IEEE Transactions on Power Electronics*, vol. 26, no. 3, pp. 786–797, Mar. 2011.

[2] Y. Yang, K. Zhou, H. Wang, F. Blaabjerg, D. Wang, and B. Zhang, "Frequency adaptive selective harmonic control for grid-connected inverters," *IEEE Transactions on Power Electronics*, vol. 30, no. 7, pp. 3912–3924, Jul. 2015.

[3] M. Castilla, J. Miret, J. Matas, L. G. d. Vicuna, and J. M. Guerrero, "Linear current control scheme with series resonant harmonic compensator for single-phase grid-connected photovoltaic inverters," *IEEE Transactions on Industrial Electronics*, vol. 55, no. 7, pp. 2724–2733, Jul. 2008.

[4] P. M. d. Almeida, J. L. Duarte, P. F. Ribeiro, and P. G. Barbosa, "Repetitive controller for improving grid-connected photovoltaic systems," *IET Power Electronics*, vol. 7, no. 6, pp. 1466–1474, Jun. 2014.

[5] A. Reznik, M. G. Simes, A. Al-Durra, and S. M. Muyeen, "Filter design and performance analysis for grid-interconnected systems," *IEEE Transactions on Industry Applications*, vol. 50, no. 2, pp. 1225–1232, Mar. 2014.

[6] J. Scoltock, T. Geyer, and U. Madawala, "Model predictive direct current control for a grid-connected converter: LCL-filter versus L-filter," in *IEEE International Conference on Industrial Technology (ICIT)*, Feb. 2013, pp. 576–581.

[7] K. A. E. W. Hamza, H. Linda, and L. Cherif, "LCL filter design with passive damping for photovoltaic grid connected systems," in *6th International Renewable Energy Congress (IREC)*, Mar. 2015, pp. 1–4.

[8] P. A. Dahono, "A control method to damp oscillation in the input LC filter," in *IEEE 33rd Annual IEEE Power Electronics Specialists Conference. Proceedings*, vol. 4, 2002, pp. 1630–1635.

[9] J. Dannehl, F. W. Fuchs, S. Hansen, and P. B. Thogersen, "Investigation of active damping approaches for PI-based current control of grid-connected pulse width modulation converters with LCL filters," *IEEE Transactions on Industry Applications*, vol. 46, no. 4, pp. 1509–1517, Jul. 2010.

[10] R. J. Vaccaro, "Tracking Systems," in *Digital Control: A State-Space Approach*. Mcgraw-Hill College, Jan. 1995, pp. 342–348.

[11] R. J. Vaccaro, "Observers," in *Digital Control: A State-Space Approach*. Mcgraw-Hill College, Jan. 1995, pp. 265–272.

[12] H.-c. Chen and P.-t. Cheng, "An active damping technique for multiple grid-connected converters," in *IEEE 3rd International Future Energy Electronics Conference and ECCE Asia (IFEEC - ECCE Asia)*, Jun. 2017, pp. 561–566.

[13] J. Wang, J. D. Yan, L. Jiang, and J. Zou, "Delay-dependent stability of single-loop controlled grid-connected inverters with LCL filters," *IEEE Transactions on Power Electronics*, vol. 31, no. 1, pp. 743–757, Jan. 2016.

[14] W. Yao, Y. Yang, X. Zhang, F. Blaabjerg, and P. C. Loh, "Design and analysis of robust active damping for LCL filters using digital notch filters," *IEEE Transactions on Power Electronics*, vol. 32, no. 3, pp. 2360–2375, Mar. 2017.

[15] R. Teodorescu, F. Blaabjerg, U. Borup, and M. Liserre, "A new control structure for grid-connected LCL PV inverters with zero steady-state error and selective harmonic compensation," in *Nineteenth Annual IEEE Applied Power Electronics Conference and Exposition (APEC)*, vol. 1, 2004, pp. 580–586 Vol.1.